



# Miniaturized DNA amplification platform with soft-lithographically fabricated continuous-flow PCR microfluidic device on a portable temperature controller

Madhusudan B. Kulkarni<sup>1</sup> · Sanket Goel<sup>1</sup>

Received: 21 April 2021 / Accepted: 22 July 2021 / Published online: 27 July 2021  
© The Author(s), under exclusive licence to Springer-Verlag GmbH Germany, part of Springer Nature 2021

## Abstract

Polymerase chain reaction (PCR) is commonly used to amplify and quantify the nucleic acid segments typically using a benchtop thermocycler. To automate, integrate, and miniaturize the PCR process, several strategies have been studied in a microfluidic environment. Among them, continuous-flow-based microfluidic PCR allows fast thermal cycling using minuscule volume, in a minimal reaction time with multiplexing. The objective was to develop a microfluidic device with a soft-lithographically fabricated continuous-flow serpentine microchannel for DNA amplification executed on a separately designed portable, easy-to-use, low-cost, automated, and miniaturized temperature controller platform (TCP). Direct laser writer (DLW) was used for developing a master on glass using a dry-film photoresist (DFR). Further, a PDMS-based microfluidic device, with dimensions 30 (L) × 0.32 mm<sup>2</sup> (W) × 35 μm (H), was developed which was bonded on glass using oxygen plasma. The portable device exhibits key features of live data streaming using an IoT platform enabling easy data accessing, monitoring and storage onto the smartphone. The temperature sensitivity of the device was ± 0.5 °C and the maximum achievable temperature was 300 °C. The microfluidic device was placed on TCP. A 20 μL of reaction volume was introduced using an automated syringe pump at various flow rates. As a proof-of-concept, the rat *GAPDH* gene of the 594-base pair was successfully amplified on the proposed platform which was validated using the gel electrophoresis method. Finally, the results obtained from the proposed device were compared with the conventional thermocycler which showed promising performance and novelty exists in the significant reduction of required amplification time with good device efficiency and low-power consumption.

**Keywords** Continuous-flow polymerase chain reaction (CF-PCR) · Microfluidics · Polydimethylsiloxane (PDMS) · Direct laser writer (DLW) · Dry-film photoresist (DFR) NodeMCU · Temperature controller platform (TCP)

## 1 Introduction

Miniaturization plays a fundamental role towards innovations in numerous biomedical diagnostics, and biological, drug-delivery, sensing, wearable, and implantable devices, and has led to the realization of micro total analysis systems (μTAS) or lab-on-a-chip (LoC) platforms (Ohno et al.

2008; Pol et al. 2017). Significant benefits for miniaturization include enhanced analytical performance, reduction of reagents volume, device size, rapid results, cost, and capability to integrate several ancillary components for fluid manipulation, detection, and analysis (Ren et al. 2014). Besides, most of the diagnostic analyses are based on traditional approaches which are limited to centralized laboratories. The associated shortcomings with the conventional procedure, such as consumption of more time/power, manual process, the specific need of equipment, and macro-scale sample (Cui et al. 2015), have made them more complicated and expensive. This has led to the increasing popularity of the miniaturized point-of-care testing (POCT) platform (Hu et al. 2016) armed with microfluidic devices (Ding et al. 2015; Nagai and Fuchiwaki 2015).

✉ Sanket Goel  
sgoel@hyderabad.bits-pilani.ac.in

Madhusudan B. Kulkarni  
madhusudankulkarni405@gmail.com

<sup>1</sup> MEMS, Microfluidics, and NanoElectronics (MMNE) Lab,  
Department of Electrical and Electronics Engineering,  
Birla Institute of Technology and Science (BITS) Pilani,  
Hyderabad Campus 500078, Telangana, India

Microfluidics is a study to manipulate and control the minuscule volume of fluid, even down to femtoliter, in the custom-fabricated microchannels and microreactors. Microfluidic systems have promising applications in chemical analysis, biological analysis, nanoparticle synthesis, cooling of Integrated Circuits (ICs), integrated optics, and so on (Kulkarni et al. 2021a; Beaulieu et al. 2017; Kulkarni and Goel 2020a; Li et al. 2011). The capability of microfluidic devices to perform measurements from such small volumes of complex liquids with efficacy and rapidity, without the necessity of a trained operator, has been considered as the supreme powerful application of Lab-on-a-Chip (LOC) technologies (Erickson and Li 2004; Manage et al. 2011). The microfluidic portable analysis systems, conducting the analytical assays at a remote location or a patient's locality, have a large demand in the biomedical and pharmaceutical industry (Cui and Wang 2019; Azizipour et al. 2020; Qiu et al. 2019).

A polymerase chain reaction (PCR) plays a significant mechanism in amplifying nucleic acid. It allows increasing the copies of particular DNA and to identify a minuscule amount of template DNA from distinct kinds of species (Mullis et al. 1992). During PCR, DNA, primers, nucleotides, and enzyme undergo three temperature regions to complete denaturation (94 °C), annealing (58 °C), and extension (72 °C) processes (Zhang and Jiang 2016). PCR is based on three simple steps required for any DNA synthesis reaction: denaturation of the template into single strands; annealing of primers to each original strand for new strand synthesis; and extension of the new DNA strands from the primers. However, most PCR quantifications are conducted on a classical PCR thermocycler which possesses more thermal mass and requires a higher volume of reaction sample, leading to a slower and tedious process (Law et al. 2014). To overcome the limitations of the conventional PCR apparatus, the microfluidic PCR device has an extensive variety of benefits, primarily for point-of-care applications (Kulkarni and Goel 2020b; Bruijns et al. 2016).

Microfluidic PCR devices can be classified into two classes: static-based PCR and dynamic-flow-based PCR. In 1993, Northrup et al. (1995a) proposed the static microfluidic PCR reactor for nucleic acid quantification. Later on, it has been emulated by other research groups, with diverse microchannel size, design, overall dimension, quantification time and integrated with other analytical features (Northrup et al. 1995b). This static PCR was a miniaturized version of the conventional PCR allowing a small reaction volume ranging from a few  $\mu\text{L}$  to nL, with fast thermal cycling. However, the evaporation of the reaction mixture becomes a challenging factor when the micro reservoir size is scaled down. Thus, this method deficits flexible modification for the temperature cycling rate (Giordano et al. 2001).

The dynamic-flow microfluidic PCR, originally introduced by Nakano et al. in 1994, works on a continuous-flow-based time-space domain wherein, the temperature remains fixed and the reaction sample flows around the three PCR zones. In 1998, the dynamic-flow-based microfluidic PCR was initiated by Kopp et al. (1998). Because of the huge demand for microfluidic PCR devices, many researchers were active in developing low-cost dynamic-flow microfluidic devices used in biomedical analysis. Tachibana et al. (2015) reported a new autonomous disposable plastic-based microfluidic PCR chip for quantitative detection of pathogenic microorganisms using the fluorescence-based validation technique. Snodgrass et al. (2016) demonstrated an integrated, portable, solar thermal PCR device targeted towards the diagnosis of Kaposi's sarcoma naming the system as KS-Detect. Such devices were shown to be fabricated using various techniques such as soft lithography (Puneeth et al. 2021), 3D printer (Bhaiyya et al. 2021), UV direct laser writer (Srikanth et al. 2020), CO<sub>2</sub> laser (Pal et al. 2021), and photolithography (Dungchai et al. 2009). Different substrate materials, such as silicon (Etchart et al. 2008), glass (Tiwari et al. 2020), quartz (Riesch et al. 2008), polymer (Kulkarni et al. 2021b) and ceramic (Natarajan and Humenik 2006), were utilized.

The main motivation here is that in the existing methods, there are many challenges such as more reaction time, high reaction volume, device efficiency, low-power consumption, requires human intervention, and are expensive, furthermore, these devices lack advanced technology for real-time data monitoring with geotagging facilities. The various advantages of the proposed device over the existing technologies such as reduced amplification time, minimum reaction volume, device efficiency, temperature sensitivity, low-power consumption, low cost, and real-time data logging with Bluetooth and IoT connected to a smartphone. The existing problem can be overcome by integrating altogether on a single platform making it more versatile.

In this work, a continuous-flow-based microfluidic device, with serpentine microchannel, has been fabricated using PDMS-glass-based soft-lithographical process, wherein the master was developed using Direct Laser Writing (DLW)-based photolithography. The objective is to develop a low-cost, portable, easy-to-use, low-powered, automated, integrated, and miniaturized temperature controller system used for the continuous-flow-based DNA amplification process. The device was integrated on a self-designed portable and automated temperature controller platform (TCP) for attaining desired temperature zones involved during PCR. TCP was automated and integrated with NodeMCU, to process, control, and monitor the custom-made cartridge heater and k-type thermocouple sensor. Further, TCP was armed with a live data streaming facility with geotagging. All the essential electronic components were integrated on a single PCB

and placed in 3D-printed housing. As a proof-of-principle, the rat *GAPGH* gene was effectively quantified with a fragment size of 594-base pair on the proposed miniaturized temperature-controlling platform.

## 2 Materials and methods

### 2.1 Chemicals and apparatus

SeaKem LE Agarose, Acetic acid, Tris base buffer, Sodium carbonate, Ethidium bromide (EtBr), and Corning Microscope slides (75 mm × 50 mm) were purchased from Sigma-Aldrich. The primers and templates were obtained from the Department of Pharmacy, BITS-Pilani, Hyderabad Campus. Table 1 shows the primer sequence of the template DNA to be amplified. DreamTaq Green PCR 2X Master mix was purchased from ThermoScientific, Invitrogen 1 Kb Plus DNA Ladder was purchased ThermoFisher Scientific. SYBR green-I Nucleic-A was procured from SR Life sciences solutions, Dow Corning Sylgard 184 Silicone Elastomer was purchased from Prabha Trade Impex Pvt. Ltd.

Veriti™ 96-Well Thermal Cycler was purchased from SR Life Science Solutions (Thermoveriti), Gel electrophoresis, and Gel-doc systems were purchased from BioBee Tech (Bangalore, India). A customized cartridge heater was purchased from Ragatiya heaters, Mumbai, India. An automated Syringe pump (HO-SPF-01) was purchased from a Holmarc Opto-Mechatronics Pvt. Ltd., Kochi, India. CUTE-1MPR for Oxygen Plasma was purchased from Femto science Inc. Korea.

### 2.2 Design and fabrication of microfluidic device

The design of the master with serpentine microchannel was confirmed after rigorous analysis of the geometry with discrete parameters such as microchannel shape and size (length, width, and height). The master was designed for 30 loops using CatiaV5 software and was saved in the .dxf file format. Then, this design was converted into a G-code using DLW lazy cam software, where scalability could also be realized. The transformed file was introduced to Mach3loader software, which worked as an interface between UV laser writer and computer. The microchannel dimension was 30 (L) mm × 0.32 mm (W) × 35 μm (H) and the space

between each cycle was around 250 μm. The total microchannel length was 1020 mm. Figure 1a shows the design for the master fabricated by the UV-DLW process. Figure 1b shows the developed master on glass slides. Figure 1c shows the PDMS–glass fabricated continuous-flow microfluidic PCR device. Further, the UV direct laser writer (DLW)-based fabricated microchannel dimensions of the master were determined using Leica Optical Microscope (DM2000 LED). Figure 1d shows the dimension of micropatterns analyzed using an optical microscope.

As shown in Fig. 2, a corning glass slide of dimension 75 × 50 × 1 mm<sup>3</sup> was used as a substrate for the master which was cleaned with 65% of ethanol and dried using nitrogen gas. Then, a dry-film photoresist (DFR) was placed onto a glass slide and passed through a laminator at 110 °C to stick with it while ensuring no air bubbles. The laminated glass substrate was permitted to cool down at room temperature. Thereafter, UV direct laser, with optimized parameters such as speed, intensity, and focus level taken from our group's previously reported work (Bhaiyya et al. 2021), was exposed onto the glass substrate to acquire micropatterns. After exposure, the protecting layer of the DFR was peeled off, and it was developed by gently spraying 0.80% sodium carbonate onto the glass slides for about a duration of 45 s to 1 min. Post-cleaning, the substrate was dried using nitrogen gas. The dimension of the obtained master with serpentine microchannel was examined through an optical microscope (Leica 2000 DM). Subsequently, Sylgard 184 elastomer (PDMS)-based soft lithography was used to fabricate the microfluidic device with serpentine microchannel based on our earlier reported work (Bhaiyya et al. 2021). As PDMS material has several advantages such as optical transparency, non-planar, rapid prototyping, and simple fabrication process. But, while experimenting few shortcomings of PDMS material were noticed such as distortion of patterns and boundary region cuttings due to micro dimensions. These were overcome using proper steps while peeling off the microchannel. Finally, oxygen plasma was used for successive bonding of the peeled PDMS layer with a fresh and clean glass slide to avoid any leakage. The same PDMS-based microchannel was reused, by just cleaning it with IPA solvent a couple of times at an optimized flow rate and drying it with a hot air oven at 60 °C for 30 min and purging it with nitrogen.

**Table 1** Primer sequence of a sample

Fragment gene	Primer sequence
Rat <i>GAPDH</i> —housekeeping gene constitutively expressed, isolated from NRK-52E kidney epithelial cells, non-infectious	5'-CAGTGCCAGCCTCGTCTCAT-3' (forward) 3'-AGGGGCCATCCACAGTCTTC-5' (reverse)

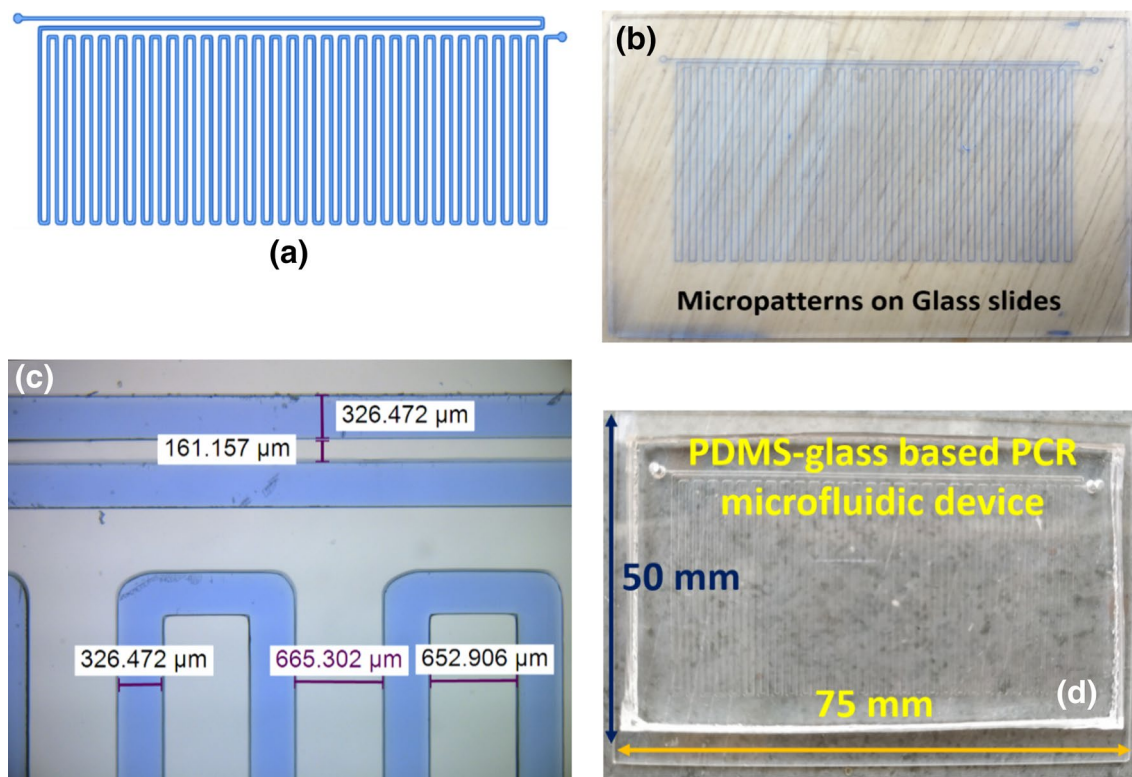


**Fig. 1** **a** Design of a serpentine microchannel. **b** Developed master on glass slides using Direct Laser Writing (DLW). **c** Microchannel width dimensions of the master analyzed using optical microscope. **d** PDMS–glass-based PCR microfluidic device

### 2.3 Development of portable and miniaturized temperature controller platform

The low-cost portable and miniaturized temperature controller platform consists of NodeMCU, self-designed switching circuitry, custom-made cartridge heater, and k-type thermocouple sensor. NodeMCU is the main heart of the entire circuit of the proposed temperature controller system. It is a microcontroller that is responsible for processing, controlling, coordinating, and monitoring the sensor and heater connected to the microcontroller as input and output, respectively. Comparatively, it is faster in processing the data and also it comes with an on-board ESP8266 (IoT) chipset when compare to other arduino boards for which external ESP8266-01 module should be used separately for IoT application. It includes firmware that runs on the ESP8266 Wi-Fi SoC from Espressif Systems, and hardware, which is based on the ESP-12 module. The ESP8266 Integrates 802.11b/g/n HT40 Wi-Fi transceiver. ThingSpeak platform is an IoT analytics platform service that lets users to collectively visualize, and analyze live data streams in the cloud. ThingSpeak utilizes Application Programming Interface (API) to store and retrieve data from things using the HTTP and MQTT protocol over the Internet or via a Local Area Network. An open-source Arduino IDE ([www.arduino.cc](http://www.arduino.cc)) software is

used for instructing/coding the microcontroller. Figure 3a shows the schematic representation of a portable temperature controller system, where the platform is divided into three categories: controller unit, switching unit, and sensor and heater unit. Here, DC-DC Buck Converter (LM2596) breakout module was used to provide the desired output at the output (load) by step-down voltage from its applied input voltage. Figure 3b shows the self-designed switching circuitry comprising of BC547 (BJT) and IRF540N (MOSFET) for controlling the surplus flow of current across the load heater (Kulkarni et al. 2020a). The primary aim of designing the switching circuit is to trigger the cartridge heater and to uphold the envisaging current across the load resistive heater. The triggering of the high and low signal is executed by the PWM signal of the microcontroller connected to the base terminal of the transistor. The K-type thermocouple sensor is used as a feedback loop responsible for measuring the real-time values which send the instructions to the microcontroller for recording and monitoring the temperature across the copper heating block at evenly spaced time intervals.

The device uses a custom-made tubular heater designed using high grade-16 stainless steel (SS) material (Kulkarni et al. 2020b). With a length of 25 mm and a diameter of 3 mm, the heater operates with an input voltage of 12 V and



**Fig. 2** Device fabrication steps involved in the development of microfluidic device using UV-DLW instrument (for master) and soft lithography process

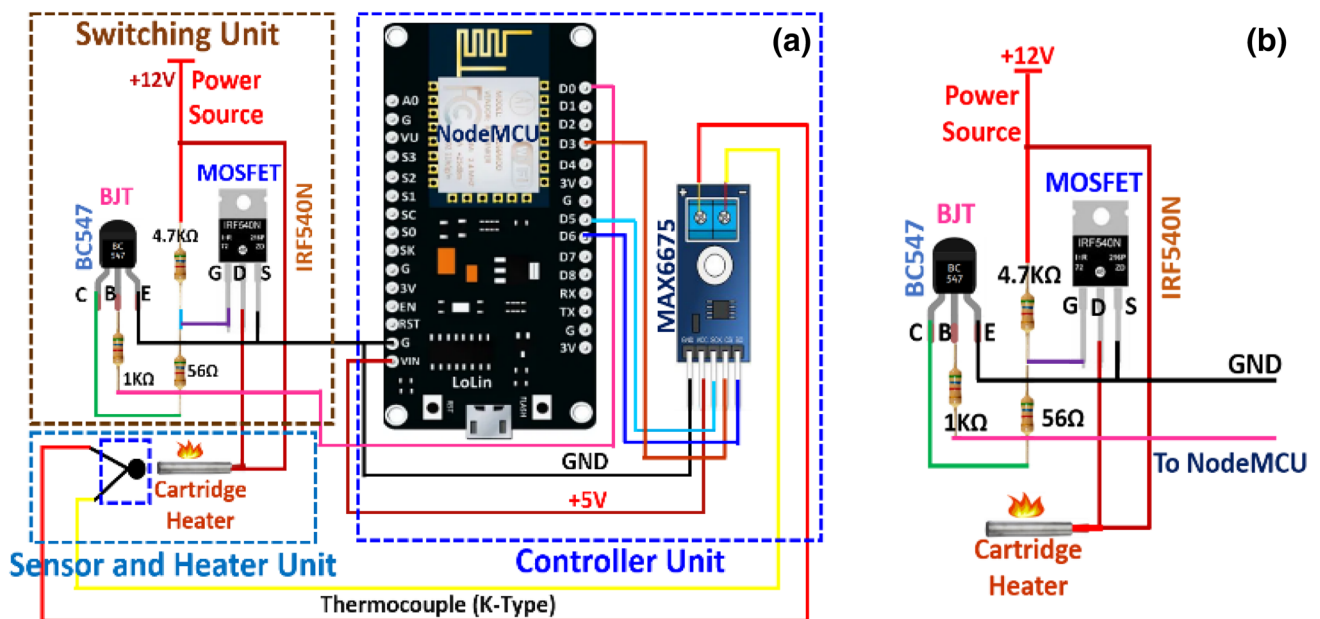
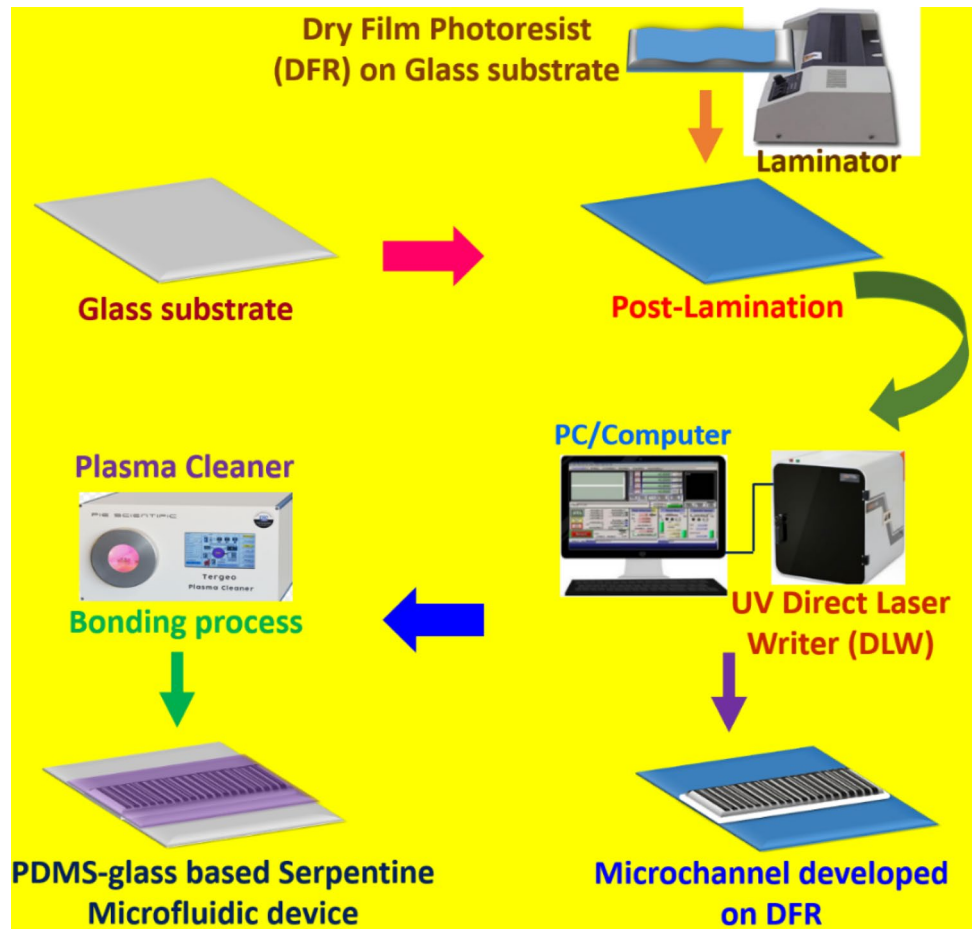


**Fig. 3** a A schematic block diagram of portable temperature controller platform. b A self-designed switching circuitry using BJT and MOSFET

requires a minimum current of 0.5 A. Along with a k-type thermocouple sensor, the MAX6675 breakout module was used to minimize the error, noise, and fluctuation during the sensing action. The breakout module was combined with a full-duplex serial peripheral interface (SPI) standards for simultaneous data transferring purposes. The device worked on an On/Off-based controller. The maximum attainable temperature was 300 °C and the temperature sensitivity of the device was  $\pm 0.5$  °C.

### 3 Results and discussions

#### 3.1 Portable temperature controller platform

Figure 4a shows the electronic components integrated and mounted onto a single PCB. Herein, the device encompasses an onboard IoT module for a live data streaming facility directly accessed and stored onto the smartphone. Figure 4b shows an image of a microfluidic device integrated with the portable temperature controller platform. Here, the microfluidic device was placed on copper heating blocks with dimensions  $80 \times 15 \times 10$  mm<sup>3</sup>. The heat sink plaster was used for better thermal crosstalk between heating blocks and the microfluidic device. The 3D-printed small reservoir was used to collect the sample from the microchannel. The complete device dimension was 105 (L)  $\times$  94 (W)  $\times$  40 (H) mm<sup>3</sup>. Figure 5 shows the ThingSpeak-based IoT platform for real-time temperature data logging.

#### 3.2 Temperature profile on PDMS–glass microchannel

The thermal IR pictures were taken using an infrared camera (Fluke PTi120) to assess the temperature profile of the microfluidic device top layer for two temperature zones involved in the PCR process: denaturation (95 °C) and annealing (65 °C). In the third step of PCR, elongation (72 °C) was obtained after attaining equilibrium from the two desired temperature zones. Herein, a calibration check of the IR camera was performed by measuring the target with the known temperature value and comparing the known vs. the measured temperature. The experiment was conducted at an ambient temperature. Herein, the environmental temperature variations can greatly affect successful DNA cycling. Further, because of the environmental changes, there was a slight variation ( $\pm 2$  °C) in the temperature range which can be noticed from the IR images. A good thermal gradient and temperature distribution were noticed on the upper surface of the microchannel. IR camera was used to observe the temperature on the top surface of the microfluidic device and it was also cross verified with the IR gun. It was checked for 2–3 iterative times where the temperature was almost the same. In Fig. 6, a higher temperature range can be easily distinguished and visualized. Figure 6 shows the three different temperature zones: (a) denaturation at 92 °C, (b) annealing at 65 °C, and (c) elongation at 72.5 °C. Further, the junction point in the IR image depicts the temperature of that particular region of the spot. The real temperature of

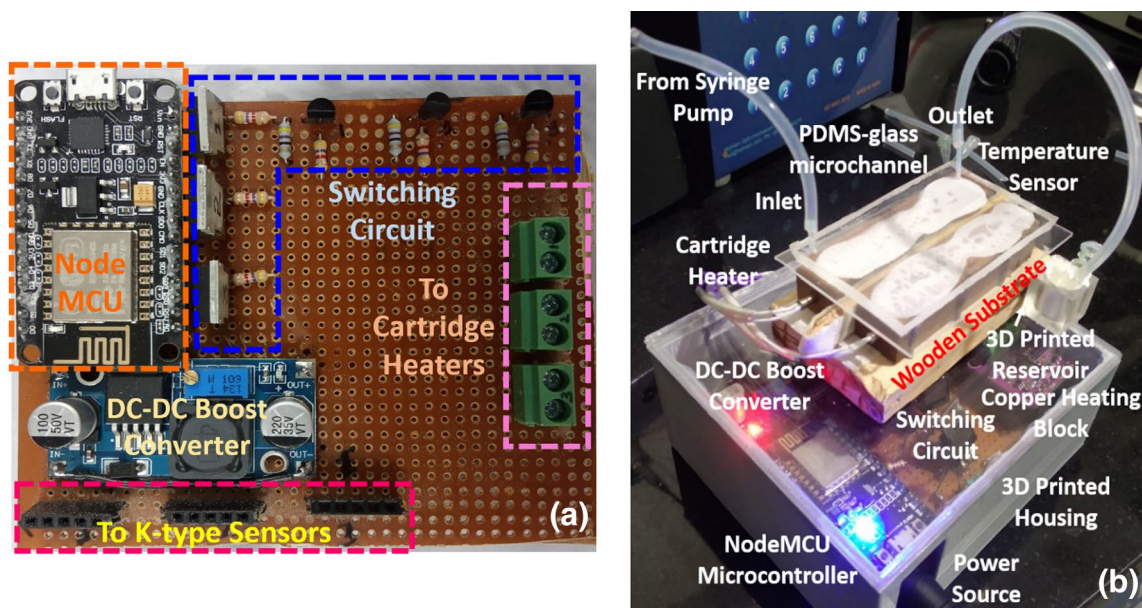


**Fig. 4** **a** An integrated electronic components on PCB. **b** A portable and miniaturized temperature controller platform with PDMS–glass microchannel

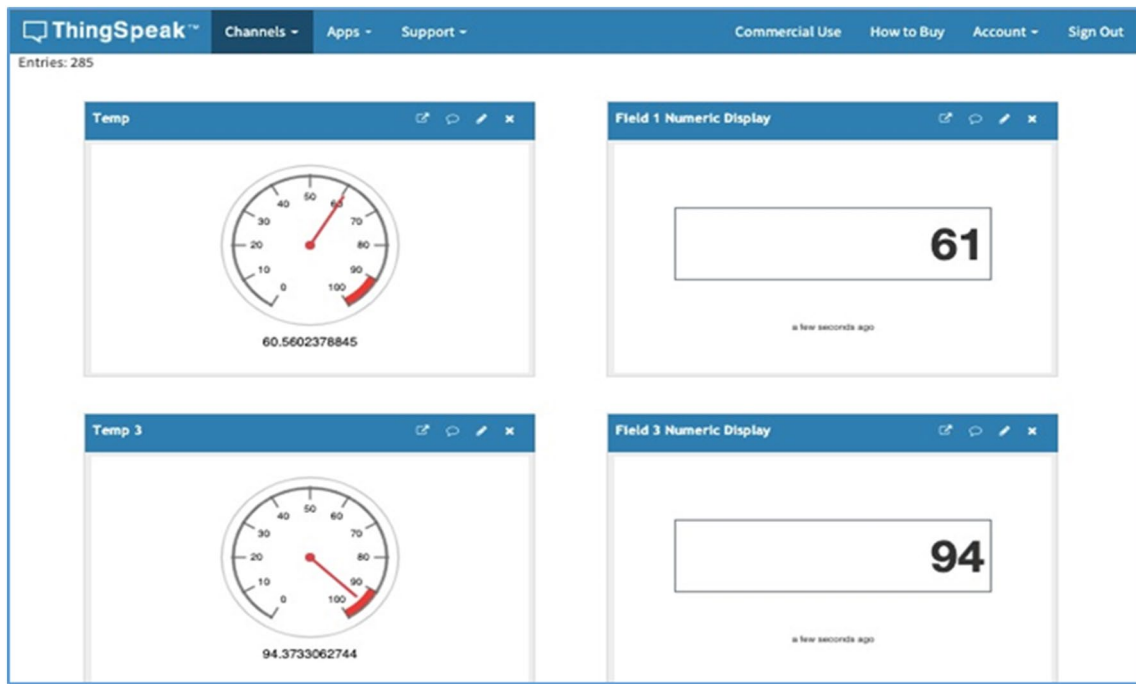


Fig. 5 ThingSpeak-based IoT platform for real-time temperature data logging

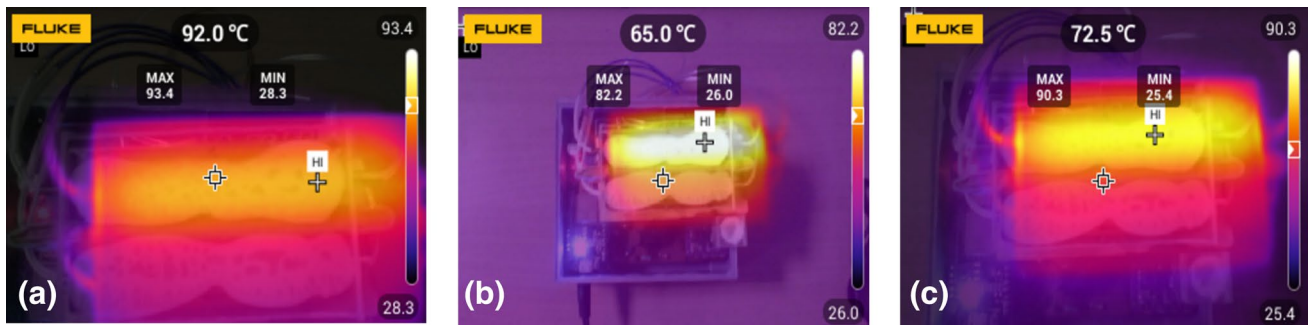


Fig. 6 Thermal images of the PDMS–glass-based PCR microfluidic device. **a** Denaturation at 92 °C. **b** Annealing at 65 °C. **c** Elongation at 72.5 °C

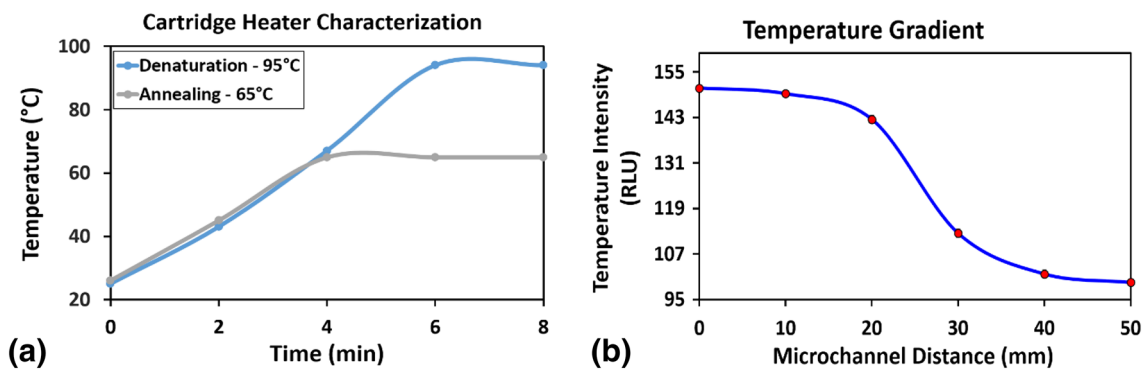


Fig. 7 **a** Time versus temperature plot for both the cartridge heaters at denaturation (95 °C) and annealing (65 °C). **b** Temperature gradient between 95 °C and 65 °C



the cartridge heater was set at an offset of  $\pm 8\text{ }^\circ\text{C}$  to attain the preferred temperature across the microfluidic device.

Figure 7a shows the time versus temperature plot for both the cartridge heaters at an applied voltage of 12 V. In addition, time dependency of the temperature can be noticed. The cartridge heater showed a good ramping response over the applied voltage. Here, the required warm-up time was around 4–5 min approximately for the entire copper blocks to reach the higher degree temperature of PCR for the thermal

cycling process. Once it reaches desired temperatures, the device performance was stable for an infinite time with the varying temperature accuracy of  $\pm 0.5\text{ }^\circ\text{C}$ . The warm-up time primarily reliant on the length of the copper heating blocks ( $80 \times 15 \times 10\text{ mm}^3$ ). Figure 7b shows the temperature gradient between denaturation ( $95\text{ }^\circ\text{C}$ ) and annealing ( $60\text{ }^\circ\text{C}$ ). A temperature gradient is a physical quantity that describes in which direction and at a certain rate the temperature changes rapidly around a specific region. Here, IR images were used

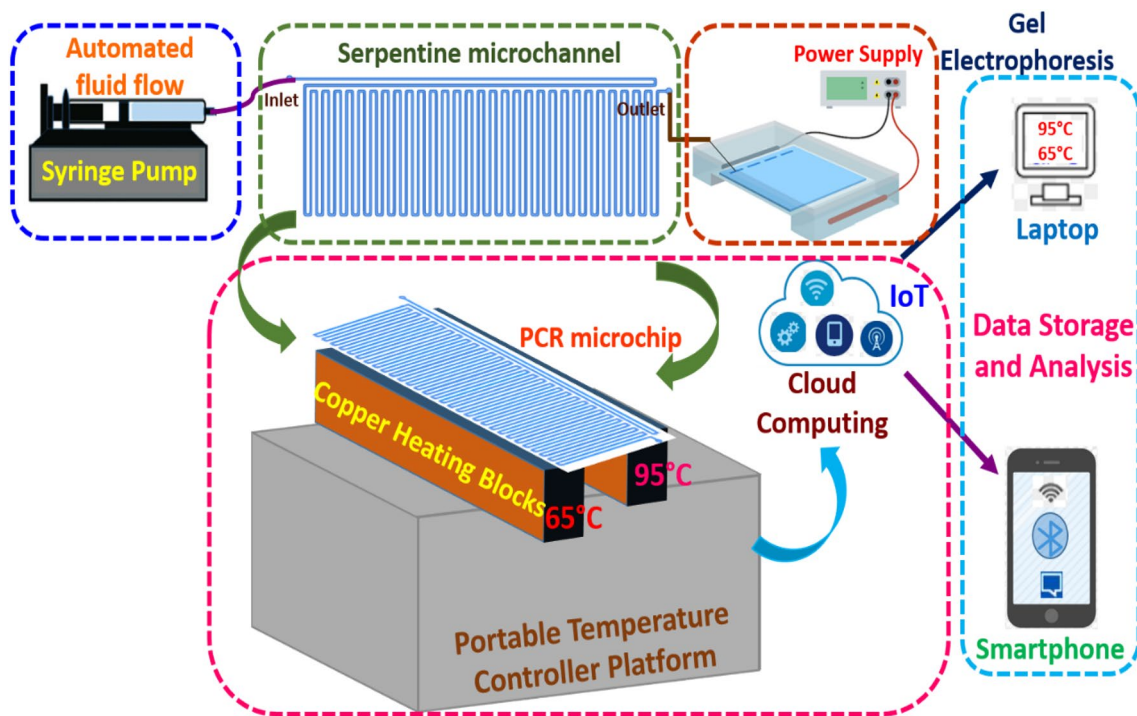
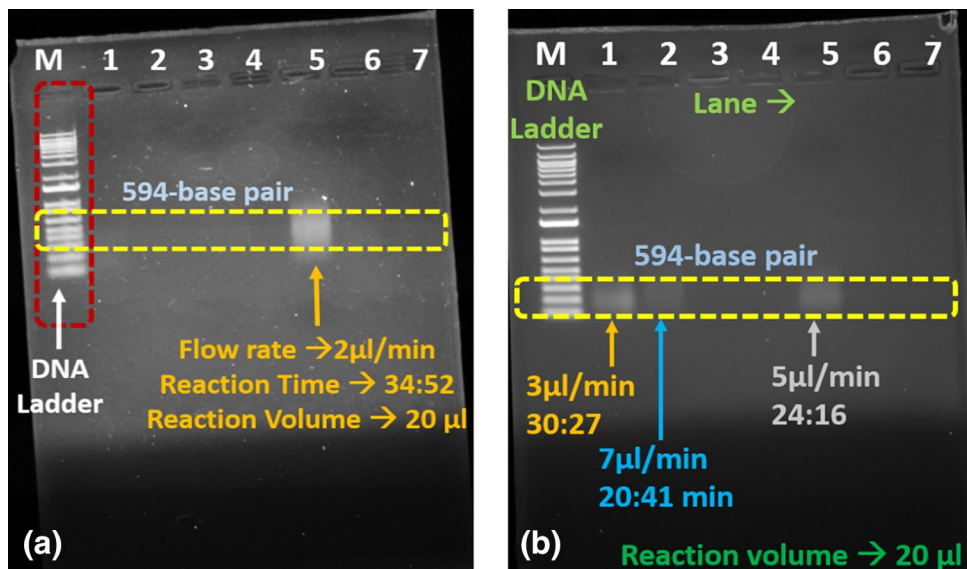


Fig. 8 Complete experimental setup of continuous-flow microfluidic PCR using a portable device

Fig. 9 a Gel electrophoresis result of PCR product on the proposed microfluidic device. Lane M: 1 kbp ladder marker, lane 5: PCR product from CF-PCR microfluidic channel for  $2\text{ }\mu\text{L}/\text{min}$ . b Lane M: 1 kbp ladder marker, lane 1, 2, and 5: PCR products with different flow rates of 3, 5, and  $7\text{ }\mu\text{L}/\text{min}$ , respectively





as a source for studying the temperature gradient between the two thermal zones by analyzing the change in intensity considering the distance of the microchannel. An ImageJ software was used to calculate the intensity of that particular thermal zone. The highest intensity was noticed across 95 °C and the lowest intensity was observed across 65 °C, determined on the microfluidic device. However, the corresponding temperature for that particular intensity value was known by the IR camera. This study was repeated 2–3 times to understand the uniformity of the temperature gradient with different IR images, wherein each time it was showing a similar response.

### 3.3 Gel electrophoresis

A PCR reaction volume of 20 µL was inserted through an external syringe pump at the inlet of the microfluidic device. After passing through the microchannel with varying speeds, the PCR product was extracted from an outlet and processed to gel electrophoresis for validation. The agarose gel electrophoresis separates the DNA molecules as per their size under the influence of electric power. Later on, a UV transilluminator was used to acquire the electrophoresis grayscale image. Furthermore, the acquired results were successfully compared to that of a traditional PCR machine. Figure 8 shows the complete experimental setup of continuous-flow microfluidic PCR using a portable device.

### 3.4 DNA amplification analysis using ImageJ software

Figure 9a illustrates the gel electrophoresis outcome at a single stream rate of 2 µL/min in 34:52 min. Figure 9b displays the gel electrophoresis results at different flow rates such as 2, 3, 5, and 7 µL/min, while no amplification was noticed at 12 and 10 µL/min. Herein, the residual time of the PCR reaction within a suitable temperature zone was dependent

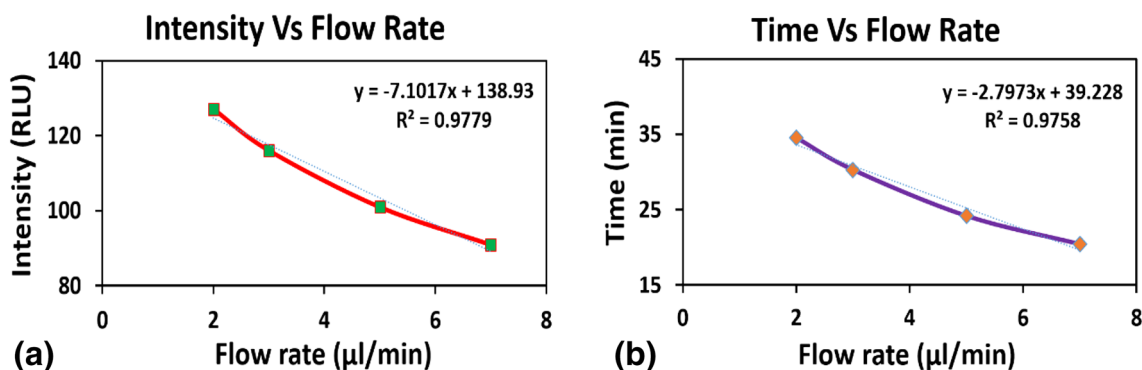
**Table 2** Analysis of DNA amplification results under different flow rates

Intensity (RLU)	Flow rate (µL/min)	Reaction time (min)
132	2	34:52
116	3	30:27
101	5	24:16
91	7	20:41

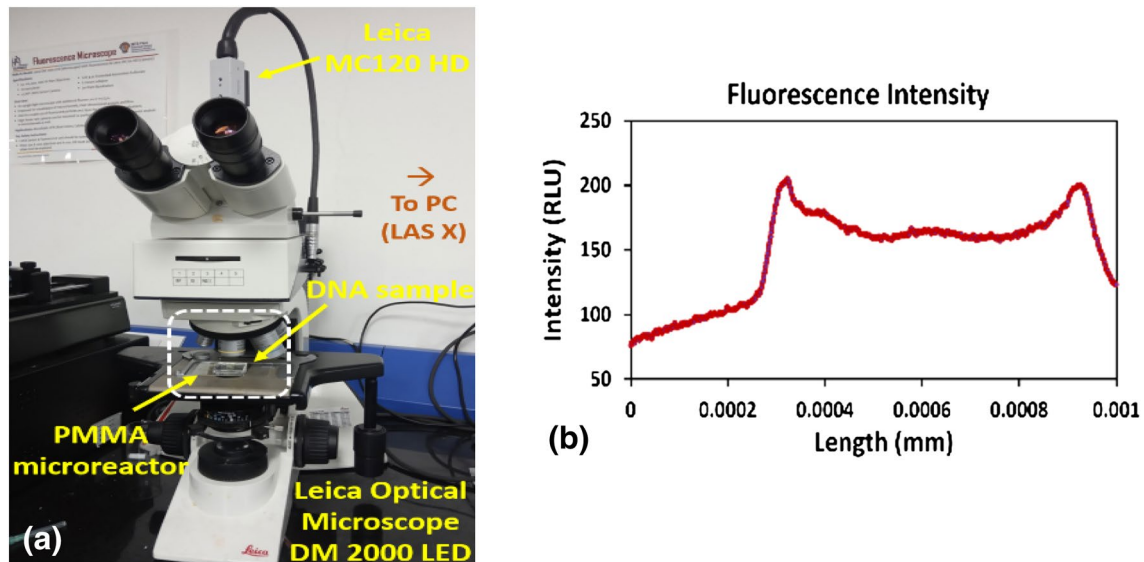
on the length and width dimensions of the microchannel and the applied stream rate. The platform was used to verify the viability of the amplification *GAPDH* gene (Cho et al. 2007), with a 10 ng/µL of template concentration and gene fragment of 594-base pair. This means that the present device is capable of carrying out a PCR reaction. Although the microchannel gained band is a little weaker, this is inevitable for flow-through-based PCRs due to the larger surface length of the serpentine channel can unexpectedly adsorb the biomolecules. Using ImageJ software, the intensity was determined by selecting the area/pixel. Finally, the obtained results were compared with the conventional Veriti™ 96-Well Thermocycler, a commercial cycler. The results indicate the portable microfluidic PCR device can be applied for preliminary on-chip amplification.

Figure 10a and b demonstrates the plots showing the variation of the intensity with flow rate and time, wherein it can be noticed that the rise in flow rate leads to a fall in reaction time and further decreases the band intensity of the PCR product. A total of three repetitions were carried out during the experimental process using ImageJ software for analyzing the results of gel electrophoresis (Hartig 2013).

Table 2 summarizes the DNA amplification results obtained at different flow rates. As can be realized, at higher flow rates (7 µL/min and 5 µL/min), the band has less intensity, while at lower flow rates (2 µL/min and 3 µL/min), the band had higher intensity. However, at a lower flow rate,



**Fig. 10** Plots illustrating **a** intensity vs flow rate and **b** time vs flow rate



**Fig. 11** **a** Intensity profiles analyzed using Leica Optical Microscope (LAS X Software). **b** Fluorescence intensity values for amplified sample

sample loss was noticed. The area/pixel value for the said intensity was around 1220 and the reaction volume of 20  $\mu\text{L}$  was used for each flow rate.

### 3.5 DNA sample intensity analysis using optical microscope

In the separate study, the behavior of the DNA sample with (amplified) and without amplified (crude) quantification on the presented platform was studied. Wherein, SYBR green-I

was used along with the sample. Further, the sample was dispensed in two small polymethyl methacrylate (PMMA) microreactor wells which were fabricated using a  $\text{CO}_2$  laser. The dimension of the PMMA reactor was  $30 \times 30 \text{ mm}^2$  with a circular section (7.5 mm diameter and 2 mm depth). Both crude and amplified DNA samples of volume 10  $\mu\text{L}$ , respectively, were introduced in these two separate microreactor wells which were placed under the optical microscope (Leica DM 2000 LED) as shown in Fig. 11a. With the help of specific Leica Application Suite X (LAS X) software, the

**Table 3** Salient features of the proposed system were compared with recent state-of-the-art continuous-flow microfluidic PCR devices

References	Parameters					
	Microchannel dimension (L $\times$ W $\times$ H)	Fabrication/material	Heating element/thermal zones	Reaction volume/time	Thermal cycles	Detection
Pal et al. (2021)	20 mm $\times$ 240 $\mu\text{m}$ (W) $\times$ 250 $\mu\text{m}$ (D)	CNC milling/PDMS	Heating resistors/three	30 $\mu\text{L}$ /NA	30	Gel electrophoresis
Fernández-Carballo et al. (2016)	46.0 $\times$ 30.9 $\times$ 0.4 mm <sup>3</sup>	Hot embossing/thermoplastic cyclo-olefin polymer	Cartridge heater/two	20 $\mu\text{L}$ /20 min	40	Fluorescence intensity
Ma et al. (2019)	76 $\times$ 52 $\times$ 1 mm <sup>3</sup>	Photolithography/PDMS	Plate heater/three	20 $\mu\text{L}$ /NA	35	Fluorescence intensity
Mavraki et al. (2011)	20 $\times$ 0.1 $\times$ 0.2 mm <sup>3</sup>	Photolithography/PCB	Integrated micro heater/three	30 $\mu\text{L}$ /45 min	30	Gel electrophoresis
Tiwari et al. (2020)	20 $\times$ 0.5 $\times$ 0.1 mm <sup>3</sup>	Toner transfer photoresist technique/PDMS	Iron box/two	33 $\mu\text{L}$ /NA	7	Gel electrophoresis
This work	30 mm $\times$ 326 $\mu\text{m}$ $\times$ 35 $\mu\text{m}$	UV direct laser writer (DLW)/soft lithography	Cartridge heater/two	20 $\mu\text{L}$ /20:41 min	30	Fluorescence intensity and gel electrophoresis

analysis of intensity profile was carried out for both the DNA samples. Further, based on the region-of-interest (ROI), the length of the particular sample was selected in the software to note the intensity profile across both samples. Herein, four experimental iterations were carried out to understand the intensity profile, and the mean value for amplified and a crude sample was 165 and 35, respectively. Therefore, from this, it was clear that the amplified DNA sample on a proposed device was showing higher intensity values when compared to the crude DNA sample. In the amplified sample, molecules were visualized in the optical microscope and no molecules were observed in the non-amplified sample. Figure 11b shows the fluorescence intensity profile for an amplified DNA sample. Herein, a high-intensity value was observed across the amplified sample and there was no intensity value observed for the crude sample. Further, confirming the amplification of DNA samples on a proposed thermal management system.

Table 3 shows the salient features of the developed system were compared with current state-of-the-art continuous-flow microfluidic PCR devices. It is evident that better DNA bands have been achieved in earlier work, however, the operation was dependent on bulky laboratory-based equipment or complicated and expensive driving mechanism, which is contradictory to the need for a portable, low-cost and standalone device. The current system provided an IoT-enabled, automated, standalone, low-power consumption, and low-cost detection system. Obtained results displayed good repeatability of amplification and further, showing good temperature sensitivity with better overall performance.

## 4 Conclusion

The present work aims to develop a microfluidic device integrated with a portable and easy-to-use temperature controller platform for nucleic acid amplification. A microfluidic device, with a serpentine microchannel, was soft-lithographically fabricated using a direct laser written (DLW) master. A temperature-controlling platform was developed wherein a nodeMCU was incorporated with a cartridge heater and thermocouple sensor for precise controlling and monitoring of the temperature. An automated and integrated temperature controller platform works with an on/off controller showing good stability, reliability, and precision. With dimensions 105 (L) × 94 (W) × 40 (H) mm<sup>3</sup>, the accuracy of the temperature controller platform was ± 0.5 °C with a maximum achievable temperature of 300 °C. The nodeMCU module has an onboard Wi-Fi facility, wherein the live data streaming can be directly accessed on a smartphone, further making the device smart and suitable for point-of-care

applications. Two temperature zones of PCR: denaturation (95 °C) and annealing (65 °C) were successfully established using a portable temperature controller. Two copper blocks were utilized as a platform to efficiently transfer the required temperature onto the microchannel. A total reaction volume of 20 µL was introduced in a microchannel via an automated syringe pump with varying flow rates. For 7 µL/min, the fastest time reaction time of 20:41 min was noticed. Faster PCR was possible although the sensitivity was reduced. The gel electrophoresis technique was utilized for the separation of DNA molecules and a gel-doc system was utilized for the validation of DNA bands. Herein, as a proof-of-concept, the *GAPDH* gene of the 594-base pair was successfully amplified with reduced reaction volume and time after comparing with the conventional PCR machine. Herein, the novelty of the proposed system is reduced reaction time (~ 20 min), low-power consumption (9 W), and low cost (~ 26\$). In addition, the proposed microdevice has the potential to be used for minimal reaction volume (< 10 µL). Because of its potential and versatility, it can be used for several purposes in the future to harness the microfluidic system for biomedical diagnostics and biochemical sensing applications. The platform is amenable to be used for several thermal-based processes such as nanoparticle synthesis, biological, and rheological applications. Work is going on to integrate the detection unit with the portable temperature controller platform for effective and efficient amplification and verification. In future studies, this microfluidic device will be upgraded to make it more controllable, allowing it to be applied to a wider field of applications.

**Acknowledgements** The authors are thankful to the Centre for Human Disease Research (CHDR), BITS-Pilani, Hyderabad Campus for providing financial support during this work. Madhusudan B Kulkarni is thankful to Tata Consultancy Services (TCS) for providing scholarship during this project. The authors are thankful to Mr. Srashti Gopal Goyal, Department of Pharmacy, BITS-Pilani, Hyderabad campus, for providing the samples and helping in the experimental setup.

## References

- Azizipour N, Avazpour R, Rosenzweig DH, Sawan M, Ajji A (2020) Evolution of biochip technology: a review from lab-on-a-chip to organ-on-a-chip. *Micromachines* 11(6):1–15. <https://doi.org/10.3390/mi11060599>
- Beaulieu LY, Logan ER, Gering KL, Dahn JR (2017) An automated system for performing continuous viscosity versus temperature measurements of fluids using an Ostwald viscometer. *Rev Sci Instrum.* <https://doi.org/10.1063/1.4990134>
- Bhaiyya M, Pattnaik PK, Goel S (2021) Electrochemiluminescence sensing of vitamin B 12 using laser-induced graphene based bipolar and single electrodes in a 3D-printed portable system. *Microfluid Nanofluid* 25(41):1–8. <https://doi.org/10.1007/s10404-021-02442-x>

- Brujins B, van Asten A, Tiggelaar R, Gardeniers H (2016) Microfluidic devices for forensic DNA analysis: a review. *Biosensors* 6(3):1–35. <https://doi.org/10.3390/bios6030041>
- Cho CH, Cho W, Ahn Y, Hwang SY (2007) PDMS–glass serpentine microchannel chip for time domain PCR with bubble suppression in sample injection. *J Micromech Microeng* 17(9):1810–1817. <https://doi.org/10.1088/0960-1317/17/9/009>
- Cui P, Wang S (2019) Application of microfluidic chip technology in pharmaceutical analysis: a review. *J Pharm Anal* 9(4):238–247. <https://doi.org/10.1016/j.jpha.2018.12.001>
- Cui F, Rhee M, Singh A, Tripathi A (2015) Microfluidic sample preparation for medical diagnostics. *Annu Rev Biomed Eng* 17:267–286. <https://doi.org/10.1146/annurev-bioeng-071114-040538>
- Ding X, Srinivasan B, Tung S (2015) Development and applications of portable biosensors. *J Lab Autom* 20(4):365–389. <https://doi.org/10.1177/2211068215581349>
- Dungchai W, Chailapakul O, Henry CS (2009) Electrochemical detection for paper-based microfluidics. *Anal Chem* 81(14):5821–5826. <https://doi.org/10.1021/ac9007573>
- Erickson D, Li D (2004) Integrated microfluidic devices. *Anal Chim Acta* 507(1):11–26. <https://doi.org/10.1016/j.aca.2003.09.019>
- Etchart I, Chen H, Dryden P, Jundt J, Harrison C, Hsu K, Marty F, Mercier B (2008) MEMS sensors for density-viscosity sensing in a low-flow microfluidic environment. *Sens Actuators A Phys* 141(2):266–275. <https://doi.org/10.1016/j.sna.2007.08.007>
- Fernández-Carballo BL, McGuinness I, McBeth C, Kalashnikov M, Borrós S, Sharon A, Sauer-Budge AF (2016) Low-cost, real-time, continuous flow PCR system for pathogen detection. *Biomed Microdevices* 18(2):1–10. <https://doi.org/10.1007/s10544-016-0060-4>
- Giordano BC, Ferrance J, Swedberg S, Hühmer AFR, Landers JP (2001) Polymerase chain reaction in polymeric microchips: DNA amplification in less than 240 seconds. *Anal Biochem* 291(1):124–132. <https://doi.org/10.1006/abio.2000.4974>
- Hartig SM (2013) Basic image analysis and manipulation in imageJ. *Curr Protoc Mol Biol*. <https://doi.org/10.1002/0471142727.mb1415s102>
- Hu J, Cui X, Gong Y, Xu X, Gao B, Wen T, Lu TJ, Xu F (2016) Portable microfluidic and smartphone-based devices for monitoring of cardiovascular diseases at the point of care. *Biotechnol Adv* 34(3):305–320. <https://doi.org/10.1016/j.biotechadv.2016.02.008>
- Kopp MU, Luechinger MB, Manz A (1998) Continuous flow PCR on a chip. *Micro Total Anal Syst* 98:7–10. [https://doi.org/10.1007/978-94-011-5286-0\\_2](https://doi.org/10.1007/978-94-011-5286-0_2)
- Kulkarni MB, Goel S (2020a) Microfluidic devices for synthesizing nanomaterials—a review. *Nano Express* 1(1):1–30. <https://doi.org/10.1088/2632-959X/abcca6>
- Kulkarni MB, Goel S (2020b) Advances in continuous-flow based microfluidic PCR devices—a review. *Eng Res Express*. <https://doi.org/10.1088/2631-8695/abd287>
- Kulkarni MB, Enaganti PK, Amreen K, Goel S (2020a) Integrated temperature controlling platform to synthesize ZnO nanoparticles and its deposition on Al-foil for biosensing. *IEEE Sens J*. <https://doi.org/10.1109/JSEN.2021.3053642>
- Kulkarni MB, Yashas PKE, Amreen K, Goel S (2020b) Internet of Things enabled portable thermal management system with microfluidic platform to synthesize MnO<sub>2</sub> nanoparticles for electrochemical sensing. *Nanotechnology* 31(42):1–8. <https://doi.org/10.1088/1361-6528/ab9ed8>
- Kulkarni MB, Enaganti KV, Khairunnisa P, Jayabalan A (2021a) Smartphone enabled miniaturized temperature controller platform to synthesize nio/cuo nanoparticles for electrochemical sensing and nanomicelles for ocular drug delivery applications. *Biomed Microdevices*. <https://doi.org/10.1007/s10544-021-00567-y>
- Kulkarni MB, Goyal S, Dhar A, Sriram D, Goel S (2021b) Miniaturized and IoT enabled continuous-flow based microfluidic PCR device for DNA amplification. *IEEE Trans Nanobiosci* 1241:1–8. <https://doi.org/10.1109/tnb.2021.3092292>
- Law JWF, Mutalib NSA, Chan KG, Lee LH (2014) Rapid methods for the detection of foodborne bacterial pathogens: principles, applications, advantages and limitations. *Front Microbiol* 5:1–20. <https://doi.org/10.3389/fmicb.2014.00770>
- Li Y, Zhang C, Xing D (2011) Fast identification of foodborne pathogenic viruses using continuous-flow reverse transcription-PCR with fluorescence detection. *Microfluid Nanofluid* 10(2):367–380. <https://doi.org/10.1007/s10404-010-0675-3>
- Ma SY, Chiang YC, Hsu CH, Chen JJ, Hsu CC, Chao AC, Lin YS (2019) Peanut detection using droplet microfluidic polymerase chain reaction device. *J Sens*. <https://doi.org/10.1155/2019/4712084>
- Manage DP, Morrissey YC, Stickel AJ, Lauzon J, Atrazhev A, Acker JP, Pilarski LM (2011) On-chip PCR amplification of genomic and viral templates in unprocessed whole blood. *Microfluid Nanofluid* 10(3):697–702. <https://doi.org/10.1007/s10404-010-0702-4>
- Mavraki E, Moschou D, Kokkoris G, Vourdas N, Chatzandroulis S, Tserepi A (2011) A continuous flow  $\mu$ PCR device with integrated microheaters on a flexible polyimide substrate. *Procedia Eng* 25:1245–1248. <https://doi.org/10.1016/j.proeng.2011.12.307>
- Mullis K, Faloona F, Scharf S, Saiki R, Horn G, Erlich H (1992) Specific enzymatic amplification of DNA in vitro: the polymerase chain reaction. 1986. *Biotechnology* 24(1):17–27
- Nagai H, Fuchiwaki Y (2015) Portable microfluidic system for rapid genetic testing. *Electron Commun Jpn* 98(12):1–6. <https://doi.org/10.1002/ecj.11753>
- Natarajan G, Humenik JN (2006) 3D ceramic microfluidic device manufacturing. *J Phys Conf Ser* 34(1):533–539. <https://doi.org/10.1088/1742-6596/34/1/088>
- Northrup MA, Gonzalez C, Lehew S, Hills R (1995a) Development of a PCR-microreactor. *Micro Total Anal Syst*. [https://doi.org/10.1007/978-94-011-0161-5\\_13](https://doi.org/10.1007/978-94-011-0161-5_13)
- Northrup MA, Gonzalez C, Hadley D, Hills RF, Landre P, Lehew S, Saiki R, Sninsky JJ, Watson R, Watson R (1995b) MEMS-based miniature DNA analysis system. In: *Eurosensors IX, the 14th international conference on solid state sensors, actuators, vol 1*, pp 764–767
- Ohno KI, Tachikawa K, Manz A (2008) Microfluidics: applications for analytical purposes in chemistry and biochemistry. *Electrophoresis* 29(22):4443–4453. <https://doi.org/10.1002/elps.200800121>
- Pal A, Kulkarni MB, Gupta H, Ponnalagu RN, Dubey SK, Goel S (2021) Portable and autonomous device for real-time colorimetric detection: validation for phosphorous and nitrite detection. *Sens Actuators A Phys* 330:112896. <https://doi.org/10.1016/j.sna.2021.112896>
- Pol R, Céspedes F, Gabriel D, Baeza M (2017) Microfluidic lab-on-a-chip platforms for environmental monitoring. *TrAC Trends Anal Chem* 95:62–68. <https://doi.org/10.1016/j.trac.2017.08.001>
- Puneeth SB, Kulkarni MB, Goel S (2021) Microfluidic viscometers for biochemical and biomedical applications: a review. *Eng Res Express* 3:1–29. <https://doi.org/10.1088/2631-8695/abfd47>
- Qiu X, Il Shu J, Baysal O, Wu J, Qian S, Ge S, Li K, Ye X, Xia N, Yu D (2019) Real-time capillary convective PCR based on horizontal thermal convection. *Microfluid Nanofluid* 23(3):1–8. <https://doi.org/10.1007/s10404-019-2207-0>
- Ren K, Chen Y, Wu H (2014) New materials for microfluidics in biology. *Curr Opin Biotechnol* 25:78–85. <https://doi.org/10.1016/j.copbio.2013.09.004>
- Riesch C, Reichel EK, Keplinger F, Jakoby B (2008) Characterizing vibrating cantilevers for liquid viscosity and density sensing. *J Sens* 2008:1–9. <https://doi.org/10.1155/2008/697062>



- Snodgrass R, Gardner A, Jiang Li, Cheng Fu, Cesarman E, Erickson D (2016) KS-Detect—validation of solar thermal PCR for the diagnosis of Kaposi's sarcoma using pseudo-biopsy samples. *PLoS ONE* 11(1):e0147636. <https://doi.org/10.1371/journal.pone.0147636>
- Srikanth S, Dudala S, Raut S, Dubey SK, Ishii I, Javed A, Goel S (2020) Optimization and characterization of direct UV laser writing system for microscale applications. *J Micromech Microeng.* <https://doi.org/10.1088/1361-6439/ab92ea>
- Tachibana H, Saito M, Shibuya S, Tsuji K, Miyagawa N, Yamanaka K, Tamiya E (2015) On-chip quantitative detection of pathogen genes by autonomous microfluidic PCR platform. *Biosens Bioelectron* 74:725–730. <https://doi.org/10.1016/j.bios.2015.07.009>
- Tiwari SK, Bhat S, Mahato KK (2020) Design and fabrication of low-cost microfluidic channel for biomedical application. *Sci Rep* 10(1):1–14. <https://doi.org/10.1038/s41598-020-65995-x>
- Zhang Y, Jiang HR (2016) A review on continuous-flow microfluidic PCR in droplets: advances, challenges and future. *Anal Chim Acta* 914:7–16. <https://doi.org/10.1016/j.aca.2016.02.006>

**Publisher's Note** Springer Nature remains neutral with regard to jurisdictional claims in published maps and institutional affiliations.